HAL open science

An unusual compound object in Yamato 793408 (H3.2-an): The missing link between compound chondrules and macrochondrules?

Jens Barosch, Dominik C Hezel, Yves Marrocchi, Andrey Gurenko, Christoph Lenting

To cite this version:

Jens Barosch, Dominik C Hezel, Yves Marrocchi, Andrey Gurenko, Christoph Lenting. An unusual compound object in Yamato 793408 (H3.2-an): The missing link between compound chondrules and macrochondrules?. Meteoritics and Planetary Science, 2020, 55 (7), pp.1458-1470. 10.1111/maps.13496 . hal-03009479

HAL Id: hal-03009479

https://hal.univ-lorraine.fr/hal-03009479v1

Submitted on 17 Nov 2020

HAL is a multi-disciplinary open access archive for the deposit and dissemination of scientific research documents, whether they are published or not. The documents may come from teaching and research institutions in France or abroad, or from public or private research centers.

L'archive ouverte pluridisciplinaire **HAL**, est destinée au dépôt et à la diffusion de documents scientifiques de niveau recherche, publiés ou non, émanant des établissements d'enseignement et de recherche français ou étrangers, des laboratoires publics ou privés.

Distributed under a Creative Commons Attribution - NonCommercial 4.0 International License

The Meteoritical Society

Meteoritics & Planetary Science 55, Nr 7, 1458–1470 (2020)
doi: 10.1111/maps.13496

An unusual compound object in Yamato 793408 (H3.2-an): The missing link between compound chondrules and macrochondrules?

Jens BAROSCH*[1], Dominik C. HEZEL[1,2], Yves MARROCCHI[3], Andrey GURENKO[3], and Christoph LENTING[1,4]

[1]Department of Geology and Mineralogy, University of Cologne, Zülpicher Str. 49b, 50674 Köln, Germany
[2]Department of Mineralogy, Natural History Museum, Cromwell Road, London SW7 5BD, UK
[3]CRPG, CNRS, Université de Lorraine, UMR 7358, Vandoeuvre-lès-Nancy 54501, France
[4]Institute of Geoscience, University of Bonn, Meckenheimer Allee 169, 53111 Bonn, Germany
*Corresponding author. E-mail: jbarosch@uni-koeln.de

(Received 20 February 2019; revision accepted 07 May 2020)

Abstract–We found a large (~2 mm) compound object in the primitive Yamato 793408 (H3.2-an) chondrite. It consists mostly of microcrystalline material, similar to chondrule mesostasis, that hosts an intact barred olivine (BO) chondrule. The object contains euhedral pyroxene and large individual olivine grains. Some olivine cores are indicative of refractory forsterites with very low Fe- and high Ca, Al-concentrations, although no ^{16}O enrichment. The entire object is most likely a new and unique type, as no similar compound object has been described so far. We propose that it represents an intermediate stage between compound chondrules and macrochondrules, and formed from the collision between chondrules at low velocities (below 1 m s^{-1}) at high temperatures (around 1550 °C). The macrochondrule also trapped and preserved a smaller BO chondrule. This object appears to be the first direct evidence for a genetic link between compound chondrules and macrochondrules. In accordance with previous suggestions and studies, compound chondrules and macrochondrules likely formed by the same mechanism of chondrule collisions, and each represents different formation conditions, such as ambient temperature and collision speed.

INTRODUCTION

Ordinary chondrites (OC) are dominated by up to 80 vol% chondrules. The mafic chondrules typically consist of olivine, pyroxene, and opaque phases such as metal, sulfide, and spinel. These phases are set in a glassy or fine-crystalline, so-called mesostasis. Chondrules have a complex formation history: in the canonical view of chondrule formation, a chondrule precursor aggregate was briefly heated to up to >2000 K, melted, and solidified subsequently in minutes to hours (Hewins et al. 2005).

Chondrules were open systems during their molten stage and interacted with their surrounding nebular gas (e.g., Tissandier et al. 2002; Libourel et al. 2006; Marrocchi and Chaussidon 2015; Friend et al. 2016; Piani et al. 2016; Soulié et al. 2017; Ebel et al. 2018; Barosch et al. 2019). The open system scenario is further supported by Marrocchi et al. (2018, 2019) and Libourel and Portail (2018), who suggested that refractory forsterites (RF)—olivines with high Ca,Al- and very low Fe-concentrations—formed from crystallization and interaction with the surrounding gas. The latter, however, is in conflict with the interpretation of Pack et al. (2004), who suggested that these refractory olivines originated from a common reservoir, that is, RF are basically xenolithic in chondrites.

Compound chondrules formed when a chondrule collided and fused together with another chondrule, fragment, or other object (Wasson et al. 1995; Arakawa and Nakamoto 2016, 2019). Such chondrule collisions might have also led to macrochondrule formation (e.g., Weyrauch and Bischoff 2012). Macrochondrules are similar in texture and composition to regular chondrules, only significantly larger (i.e., >5 mm in maximum dimension; Weisberg et al. 1988). They typically contain abundant coarse-grained olivines, while low-Ca pyroxene is often only a minor constituent—a difference to regular

© 2020 The Authors. *Meteoritics & Planetary Science* published by Wiley Periodicals LLC on behalf of The Meteoritical Society (MET)
This is an open access article under the terms of the Creative Commons Attribution-NonCommercial License, which permits use, distribution and reproduction in any medium, provided the original work is properly cited and is not used for commercial purposes.

chondrules. The mesostases of chondrules as well as macrochondrules are mostly feldspathic. Bridges and Hutchison (1997) report identical oxygen isotope compositions for macrochondrules and normal chondrules in the same meteorite. The O-isotope compositions of OC chondrules are usually ^{16}O-poor and range from approximately +2 to +5‰ in δ^{17}O and +4 to +7‰ in δ^{18}O (Scott and Krot 2014). It has been proposed that compound chondrules and macrochondrules represent various stages and/or ambient conditions of chondrule collisions, for example, macrochondrules possibly formed through collisions between molten chondrules that fully merged and grew into the exceptionally large macrochondrules (Weyrauch and Bischoff 2012; Bischoff et al. 2017; Bogdan et al. 2019). However, no unequivocal evidence for this relationship between compound and macrochondrules has so far been reported.

Ordinary chondrites occasionally contain another group of large objects with diameters above 5 mm. These clasts (Bridges and Hutchison 1997) represent a highly diverse group: they range from clearly xenolithic, chondritic fragments (e.g., impact melt clasts) to chemically fractionated objects with mineralogies and bulk compositions different from most chondrules. Therefore, these are often related to planetary differentiation processes (Hutchison et al. 1988; Bischoff et al. 1993; Bridges et al. 1995; Ruzicka et al. 1995; Bridges and Hutchison 1997; Sokol et al. 2007; Terada and Bischoff 2009; Rubin et al. 2017; Yokoyama et al. 2017; Crowther et al. 2018). Impact melt clasts represent a large subgroup of clasts and likely formed when objects from as small as chondrules up to as large as planetesimals collided. They commonly represent a different chondrite group than their host chondrites. For example, Herd et al. (2013) described an impact melt clast in the Peace River L6 chondrite that formed from LL-group chondritic material. A similar object was described in NWA 5764—a brecciated LL6 chondrite—that contains L4 clasts (Gattacceca et al. 2017). H chondrite melt clasts were detected in L (Hutchison et al. 1988) and LL chondrite hosts (Corrigan et al. 2015). Bischoff et al. (2006, and references therein) list melt clasts of various origins and formation histories. Impact melt clasts typically have microporphyritic textures, dominated by euhedral to subhedral olivine phenocrysts (e.g., Lunning et al. 2016). Pyroxenes are only observed as admixed relict grains (Metzler et al. 2011), although Fe-rich glasses of plagioclase and pyroxene-normative compositions occur frequently (e.g., Lunning et al. 2016). Many impact melt clasts completely lack any metal and sulfides (Metzler et al. 2011; Corrigan et al. 2015; Crowther et al. 2018).

Atypical objects in chondrites that are either xenolithic, rare, and/or otherwise different from the common chondritic assemblage can provide unique, and in cases even pivotal clues to understand processes in the protoplanetary disk, such as chondrule formation. Here, we study a large, 2 mm-sized fragment in the H3.2-an chondrite Yamato 793408, which has been described as being among the least equilibrated H chondrites by Kimura et al. (2002). This fragment has a peculiar texture and mineralogy and contains a well-preserved barred olivine (BO) chondrule.

METHODS

Electron Microprobe

Mineral analyses were obtained with the electron microprobe (EMP) JEOL 8900RL at the Institute of Geology and Mineralogy, University of Cologne. The accelerating voltage was set to 15 kV and the beam current to 20 nA. The ZAF algorithm was used for correction (Bence and Albee 1968). Cathodoluminescence images were taken with a black and white detector mounted on the EMP. Backscattered electron images were also taken with the EMP.

Oxygen Isotope Analyses Using Secondary Ion Mass Spectrometry

We measured the oxygen isotope compositions with a CAMECA IMS 1280 at CRPG-CNRS (Nancy, France). $^{16}O^-$, $^{17}O^-$, and $^{18}O^-$ ions produced by a Cs^+ primary ion beam (~15 mm, ~4 nA) were measured in multicollection mode with two off-axis Faraday cups (FC) for $^{16,18}O^-$ and the axial FC for $^{17}O^-$. To remove $^{16}OH^-$ interference on the $^{17}O^-$ peak and to maximize flatness atop the $^{16}O^-$ and $^{18}O^-$ peaks, the entrance and exit slits of the central FC were adjusted to obtain mass resolution power of ~7000 for $^{17}O^-$. A slit #1 (MRP = 2500) was used with the multicollection FC detectors. The total measurement times were 240 s (180 s measurement + 60 s pre-sputtering). We used five terrestrial standard materials (San Carlos olivine, magnetite, glass, clinopyroxene, and diopside) to define the instrumental mass fractionation (IMF) line for the three oxygen isotopes and correct the instrumental mass fractionation due to the matrix effect for the olivine, clinopyroxene, and glass. Typical count rates obtained on the San Carlos olivine standards were 2.5×10^9 cps for ^{16}O, 1.0×10^6 cps for ^{17}O, and 5.4×10^6 cps for ^{18}O. The 2σ errors were ≈0.2‰ for δ^{18}O, ≈0.4‰ for δ^{17}O, and ≈0.8‰ for Δ^{17}O (Δ^{17}O representing the deviation from the TFL, $\Delta^{17}O = \delta^{17}O - 0.52 \times \delta^{18}O$).

μ-Raman Spectroscopy

Raman spectra were obtained with a confocal Horiba HR800 Raman spectrometer equipped with an

Olympus BX41 microscope in 180° backscatter geometry and an EM-CCD detector at the Institute of Geoscience at the University of Bonn, Germany. Analyses were performed with a He-Ne laser (632.81 nm) with about 100 mW laser output power, a 100× objective, a 600 grooves/mm grating, a confocal hole of 500–1000 μm, and a spectrometer entrance slit width of 100 μm, yielding a spectral resolution of approximately 3.5 cm^{-1}. Prior to analysis, the spectrometer was calibrated with an Si standard. Spectra of samples were then measured for 3 × 10 s, their relative intensities were corrected with a white light source, and a fifth-order polynomial was fitted for background subtraction.

RESULTS

Petrography

Figure 1 displays the Y-793408 section. The unusual compound object is the largest object (~2 mm) in the section. It is metal-free and hosts a BO chondrule of about 1 mm in diameter (Fig. 2). In the following, we discriminate between the BO chondrule inclusion and the surrounding host object. The mesostasis of the BO chondrule and the mesostasis of the host object appear to be identical. Both are fine-grained (nm to ~10 μm-sized), eutectic intergrowths of feldspar, pyroxene, silica, and a few tiny spinels (Fig. 3). Some BO chondrule olivines have inclusions of mesostasis-like material that sometimes even show the same mineral intergrowths as the mesostases (inset b in Fig. 2). All olivines are fractured and have subhedral to rounded shapes. The olivines in the host object are up to ~500 μm long, ~200 μm wide, and seem to free-float in its mesostasis. Most clinopyroxenes occur along the border of the host object and some are free-floating in its mesostasis. They sometimes also grew onto the olivines as well as onto the border of the BO chondrule. The pyroxenes are euhedral to subhedral and often show sector zoning and the typical pyroxene cleavage along [110] (Fig. 2). The mesostasis in the host object appears to have domains, in which the tiny minerals are oriented in the same direction. The center of the host object and the center of the BO chondrule have visible and highly localized porosities (Fig. 2).

Element Compositions of the Minerals in the Compound Object

Table 1 lists representative major and minor elements of all minerals in the compound object. All olivines—no matter whether these occur in the host object or are part of the BO chondrule—are zoned with respect to several elements: FeO has the most prominent zonation from as low as 0.8 wt% in the olivine cores to up to 8.3 wt% at their rims. Some of the individual olivines have CaO (~0.9 wt%) and Al_2O_3 (~0.2 wt%) concentrations typical of RF (Steele 1986; Pack et al. 2004). Some of these olivines are CL-active —also typical of RF—for example, the two forsterites shown in inset a of Fig. 2. Unlike the other olivines, these forsterites are unzoned and have very low FeO concentrations of 0.2 wt%.

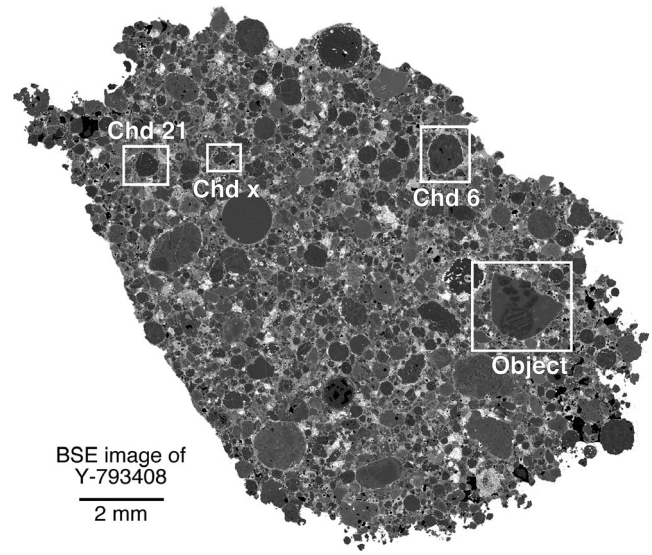

Fig. 1. BSE image overview of the Y-793408 thin section studied. The unusual compound object and three additional chondrules are shown in the boxes. We analyzed the O-isotope compositions of their mineral phases.

The pyroxenes are clinopyroxenes and are always zoned, with sometimes textbook-like developed sector zoning (Fig. 2). The oxides SiO_2 and MgO have higher concentrations in the pyroxene cores and lower concentrations at the rims ($SiO_{2\text{-core-rim}}$: 53.5–48.1 wt%; $MgO_{\text{core-rim}}$: 21.1–16.3 wt%). Inverse to this zonation, Al_2O_3, CaO, Cr_2O_3, and TiO_2 are depleted in the cores and enriched at the rims ($Al_2O_{3\text{-core-rim}}$: 3.2–10.2 wt%; $CaO_{\text{core-rim}}$: 19.0–20.5 wt%; $Cr_2O_{3\text{-core-rim}}$: 1.0–1.6 wt%; $TiO_{2\text{-core-rim}}$: 0.4–1.4 wt%). FeO (~1.9 wt%) and MnO (~0.2 wt%) do not show any zonation. The chemical compositions of other pyroxenes with less developed zonations range between the two extremes of the pyroxene. All pyroxenes have a fassaite component with Al_2O_3 ranging between 2.9 and 10.2 wt%. The FeO-concentration in these is low, between 1.8 and 2.0 wt%.

The fine-crystalline material in the host object's mesostasis and the mesostasis of the BO chondrule are compositionally identical: both are high in SiO_2 (51 wt %), Al_2O_3 (22 wt%), and CaO (14 wt%) and low in MgO (7 wt%) and FeO (2 wt%).

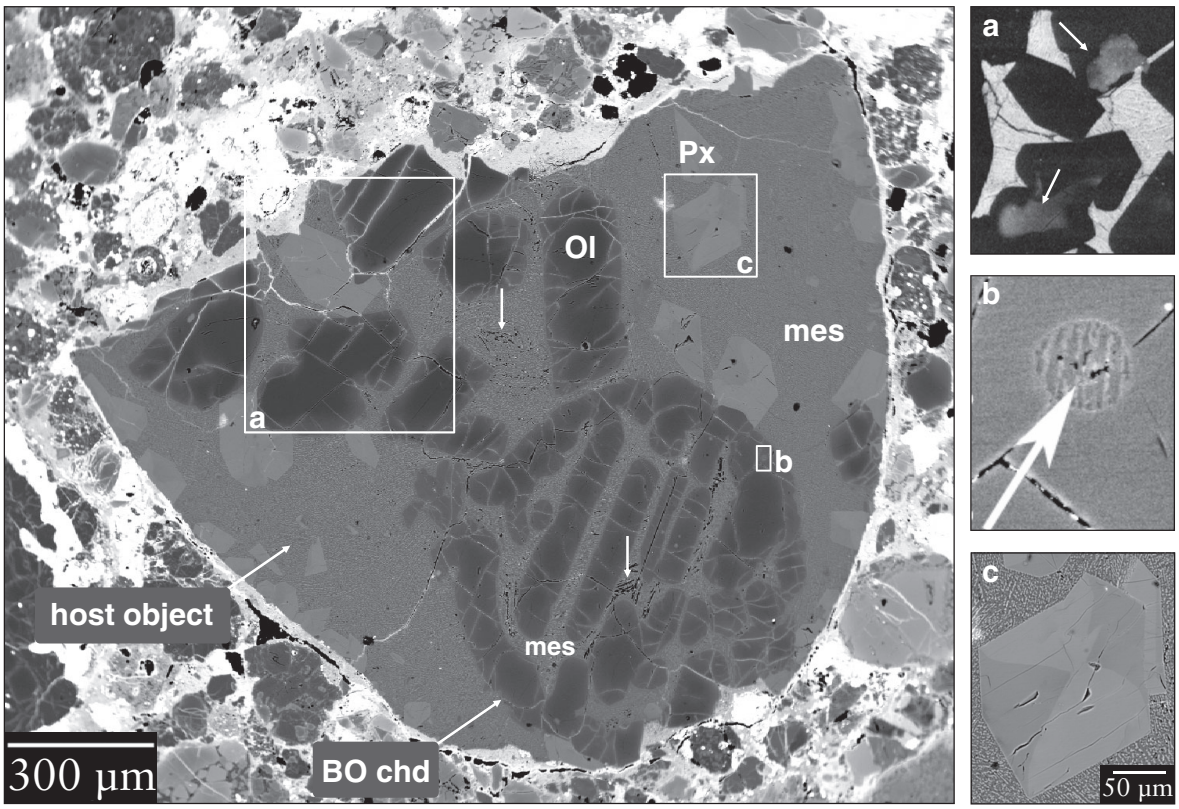

Fig. 2. BSE image of the compound object. Inset (a) is a CL image. The white cores in two olivines (white arrows) are indicative of refractory forsterites with very low Fe- and high Ca, Al-concentrations. The mesostasis (mes) in the CL-image is very bright due to the abundant presence of feldspar. Inset (b) shows the inclusion in a BO chondrule olivine. The texture and composition of this inclusion is identical to the mesostasis. Clinopyroxene shows sector zoning and [110]-cleavage (see close-up in inset c). White arrows in the center of the host object as well as the BO chondrule point at porosities.

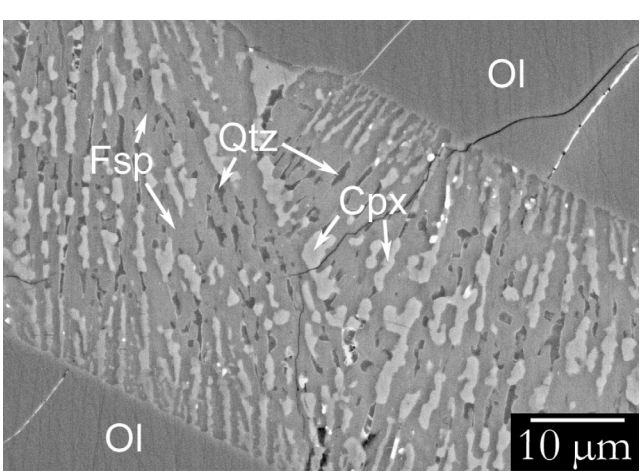

Fig. 3. BSE image enlargement of BO chondrule mesostasis. Mesostases in BO chondrule and host object appear to be petrographically and chemically identical.

Silica Is Quartz in the BO Mesostasis and Cristobalite in the Host Object's Mesostasis

The silica polymorphs in the fine-crystalline mesostases of BO chondrule and host object are different—despite otherwise almost identical petrographic and petrologic characteristics of both mesostases. The silica in the BO chondrule is quartz, while the silica in the host object is cristobalite. Representative μ-Raman spectra of the silica polymorphs in the respective mesostases are displayed in Fig. 4.

Mineral O-Isotope Compositions

We measured the O-isotope compositions of the mineral phases in the compound object and three additional chondrules (Table 2; cf. Fig. 1). Figure 5a displays the results from the compound object. The $\delta^{17}O$ compositions of the BO chondrule olivines are systematically shifted to lighter values by—on average—0.8‰, and compared to the individual olivine grains in the host object. The porphyritic pyroxenes in the host object are lighter than all olivines in the host object, in both $\delta^{17}O$ and $\delta^{18}O$, and by—on average—about 1‰. Both mesostases span a surprisingly large range, although most analyses fall roughly in between the olivine and pyroxene compositions of the host object.

Table 1. Representative mineral element compositions.

Host Object

	Ol-1	Ol-1	inc in Ol-1	Ol	Ol	Ol rim	Ol core	CL-OL	CL-OL	por Px	por Px	por Px rim	por Px core	fc Px	fc Fsp	mesA	mesA3
SiO_2	41.23	41.94	38.90	41.60	42.16	41.26	42.61	41.97	42.10	50.26	48.42	48.14	53.45	54.10	49.58	51.58	51.32
TiO_2	<d.l.	0.05	1.72	<d.l.	<d.l.	0.03	<d.l.	<d.l.	<d.l.	0.98	1.05	1.37	0.44	1.14	0.24	1.64	0.74
Al_2O_3	0.04	0.17	24.77	0.10	0.05	0.05	0.04	0.17	0.20	7.68	8.84	10.22	3.19	6.17	30.42	20.55	22.57
Cr_2O_3	0.07	0.14	0.47	0.13	0.12	0.30	0.16	0.05	0.08	1.58	1.72	1.63	1.00	0.67	<d.l.	0.37	0.27
FeO	6.62	1.05	0.36	3.38	0.87	8.27	0.81	0.19	0.19	1.77	1.85	1.86	1.91	7.37	0.47	3.28	2.60
MnO	0.05	<d.l.	<d.l.	0.03	0.03	<d.l.	<d.l.	<d.l.	0.04	0.10	0.21	0.22	0.14	0.41	<d.l.	0.20	0.17
MgO	51.72	56.00	8.83	54.05	56.12	49.85	56.62	56.68	56.50	17.01	16.78	16.32	21.10	21.62	1.00	7.08	6.30
CaO	0.11	0.65	25.07	0.49	0.56	0.30	0.41	0.88	0.76	20.60	20.85	20.47	18.99	9.79	16.40	13.63	14.27
Na_2O	<d.l.	<d.l.	<d.l.	<d.l.	<d.l.	<d.l.	<d.l.	<d.l.	<d.l.	<d.l.	<d.l.	<d.l.	<d.l.	0.15	2.02	0.63	1.49
K_2O	0.04	<d.l.	<d.l.	<d.l.	<d.l.									<d.l.	0.05		
Total	99.93	100.05	100.16	99.83	99.94	100.27	100.68	99.97	99.94	100.02	99.75	100.28	100.26	101.43	100.20	98.97	99.74

Barred olivine chondrule

	Ol	Ol	Ol rim	Ol core	Ol rim	Ol core	inc in Ol	inc in Ol	Spl	fc Px	fc Fsp	fc Silica	mesB2	mesB4
SiO_2	41.23	41.39	41.09	41.11	41.26	41.92	50.44	50.18	1.13	52.47	49.15	92.05	51.65	53.58
TiO_2	<d.l.	0.05	0.03	<d.l.	<d.l.	<d.l.	1.16	0.48	0.49	2.24	0.37	0.50	0.91	0.53
Al_2O_3	0.10	0.03	0.09	0.07	0.07	0.08	21.41	20.86	51.16	3.53	29.81	2.89	21.11	23.08
Cr_2O_3	0.26	0.14	0.18	0.21	0.08	0.19	0.50	0.38	14.09	1.54	0.12	<d.l.	0.35	0.20
FeO	4.33	7.34	4.48	3.08	5.45	2.70	0.74	2.22	13.96	5.12	0.49	0.43	2.20	1.11
MnO	0.11	0.15	0.09	0.05	0.16	0.08	<d.l.	0.09	0.13	0.37	0.05	<d.l.	0.10	0.05
MgO	53.24	51.42	53.08	54.18	52.33	54.63	3.96	10.01	17.21	17.42	1.18	0.74	7.16	5.65
CaO	0.33	0.29	0.27	0.43	0.20	0.41	15.20	12.28	0.30	18.47	16.30	2.57	14.82	13.91
Na_2O	<d.l.	<d.l.	<d.l.	<d.l.	<d.l.	<d.l.	5.67	2.06	<d.l.	0.08	2.57	0.32	0.81	1.77
K_2O	<d.l.	<d.l.					<d.l.	<d.l.	<d.l.	<d.l.	<d.l.	<d.l.		
Total	99.60	100.79	99.30	99.13	99.57	100.03	99.09	98.62	98.50	101.24	100.06	99.54	99.13	99.91

"Host object" is the object surrounding the barred olivine chondrule.

Ol = olivine; inc = inclusion; CL-OL = cathodoluminescence active olivine; por Px = porphyritic pyroxene crystals in the host object; mesA = mesostasis in the host object; mesA[3] = mean from 55 points; fc Px = fine-crystalline pyroxene in mesA; fc Fsp = fine-crystalline feldspar in mesB; Spl = spinel; mesB = BO mesostasis; mesB[2] = mean from 29 points; mesB[4] = mean from 17 points.

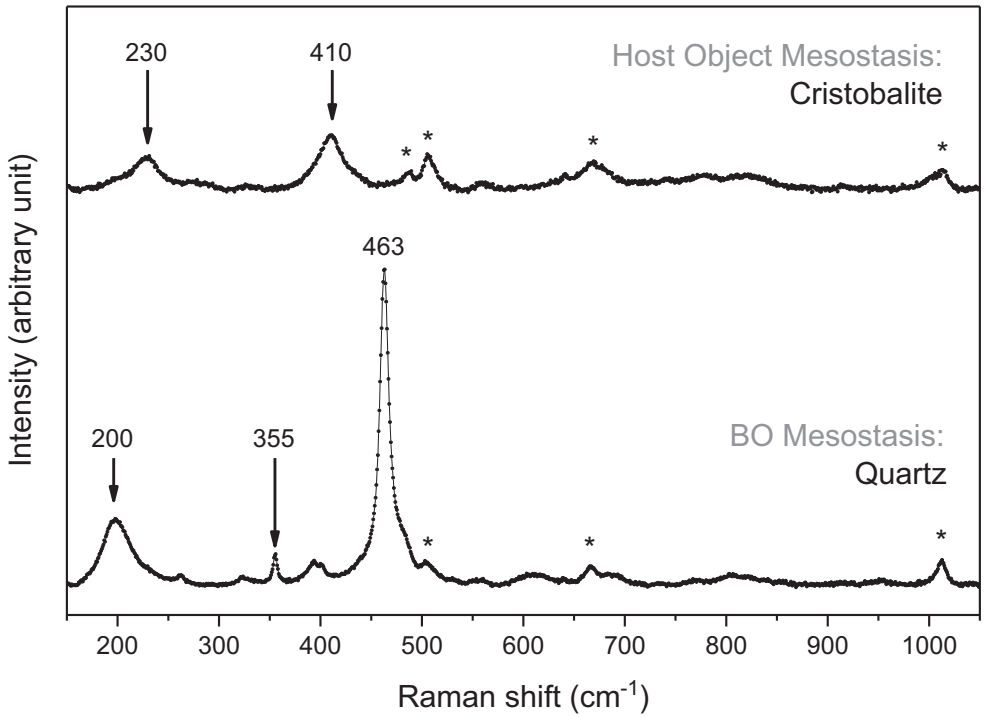

Fig. 4. Representative Raman spectra of SiO_2 phases in the host object's mesostasis and the BO mesostasis identified as cristobalite and quartz, respectively. For reference spectra of alpha-quartz, the reader is referred to Scott and Porto (1967), Etchepare et al. (1974), and Nasdala et al. (2004) and for cristobalite to Etchepare et al. (1978). Asterisks mark Raman bands originating from laser scattering of adjacent feldspar and clinopyroxene grains.

The O-isotope compositions of all minerals in the compound object are similar or slightly shifted to lighter compositions when compared to OC bulk O-isotope compositions. The opposite is observed for the O-isotope compositions of all minerals in the three other chondrules studied: all of these are shifted to slightly heavier compositions when compared to OC bulk O-isotope compositions. However, within the error, these are almost identical. The olivines in the three other chondrules are always lighter by a few permil than the pyroxenes, while the mesostasis has a roughly similar composition as pyroxene. This is a similar pattern as in the compound object. One olivine grain in chondrule 6 has a very light composition of −6.49‰ in $\delta^{17}O$ and −6.71‰ in $\delta^{18}O$ (inset in Fig. 5b).

DISCUSSION

Unusual objects, such as xenolithic clasts, are rare and highly diverse constituents of OCs (e.g., Bischoff et al. 2006, 2019). Their unusual and, in cases, unique properties often prohibit assigning these to known formation processes and places of origin. This means, studying these objects allows insights to processes and mechanisms in the early solar system that are otherwise concealed. The compound object we studied here is particularly interesting, as it appears to be of a new type. To our knowledge, no similar large, mesostasis- and refractory-rich object, hosting an intact BO inclusion, has been described before. In the following, we discuss the characteristics, origin, and evolution of the Y-793408 compound object, and compare it to other rare and unusual objects in chondrites, in particular to macrochondrules and impact melt clasts.

Mineralogy, Structure, and Petrography of the Y-793408 Compound Object

The compound object is a fragment and must have originally been significantly larger. Based on its shape, it was likely round and up to twice its current size, with an original diameter of ~5 mm. As both macrochondrules (Weyrauch and Bischoff 2012) and xenolithic clasts (Bridges and Hutchison 1997) are frequently fragmented, the broken nature of the compound object is no indication of its origin.

The occurrence of an intact BO chondrule found inside the compound object is particularly remarkable and distinctive. An equally rare clast hosting a BO chondrule was found in the Y-793241 (L6) chondrite (Prinz et al. 1984). However, this clast has a Brachina-like, Ca,Al-poor mineralogy with no individual, large

Table 2. O-isotope composition of chondrule and host object minerals.

Phase	Location	Point	δ18O	2 s.e.	$\delta^{17}O$	2 s.e.
Olivine	Host-obj	1	6.26	0.29	4.93	0.39
Olivine	Host-obj	2	4.64	0.29	3.14	0.43
Olivine	Host-obj	3	4.97	0.29	3.01	0.40
Olivine	Host-obj	4	5.92	0.29	4.19	0.39
Olivine	Host-obj	5	6.63	0.29	4.26	0.41
Olivine	Host-obj	6	5.14	0.29	3.44	0.41
Olivine	Host-obj	7	4.65	0.29	3.06	0.46
Olivine	Host-obj	8	5.31	0.29	2.49	0.45
Olivine	Host-obj	9	6.32	0.29	3.07	0.44
Olivine	Host-obj	10	4.43	0.29	1.82	0.53
Olivine	Host-obj	11	7.32	0.29	4.78	0.39
Olivine	Host-obj	12	4.81	0.29	3.23	0.45
Olivine	Host-obj	13	4.80	0.29	2.96	0.43
Olivine	Host-obj	14	5.07	0.29	2.44	0.45
Olivine	Host-obj	15	5.75	0.29	3.93	0.39
Olivine	Host-obj	16	3.84	0.29	2.78	0.47
Pyroxene	Host-obj	17	3.85	0.54	2.31	0.90
Pyroxene	Host-obj	18	4.25	0.54	2.60	0.89
Pyroxene	Host-obj	19	4.32	0.54	4.43	0.86
Pyroxene	Host-obj	20	4.26	0.54	1.90	0.97
Pyroxene	Host-obj	21	4.58	0.54	1.97	0.97
Pyroxene	Host-obj	22	5.77	0.54	3.09	0.89
Pyroxene	Host-obj	23	5.16	0.54	2.25	0.94
Pyroxene	Host-obj	24	4.11	0.54	1.89	0.94
Pyroxene	Host-obj	25	4.28	0.54	2.58	0.93
Pyroxene	Host-obj	26	4.09	0.54	3.51	0.88
Pyroxene	Host-obj	27	5.77	0.54	3.93	0.88
Mesostasis	Host-obj	39	1.20	0.48	−0.07	2.13
Mesostasis	Host-obj	40	3.22	0.29	1.70	0.58
Mesostasis	Host-obj	46	5.04	0.11	3.03	0.68
Mesostasis	Host-obj	47	4.53	0.11	3.79	0.59
Mesostasis	Host-obj	48	3.82	0.11	2.93	0.66
Mesostasis	Host-obj	49	5.78	0.10	3.08	0.67
Mesostasis	Host-obj	50	7.68	0.09	7.54	0.58
Olivine	BO	28	5.51	0.29	1.57	0.56
Olivine	BO	29	4.87	0.29	2.79	0.48
Olivine	BO	30	5.72	0.29	2.34	0.47
Olivine	BO	31	5.58	0.29	2.22	0.49
Olivine	BO	32	6.04	0.29	3.44	0.42
Olivine	BO	33	6.02	0.29	2.55	0.44
Olivine	BO	34	4.62	0.29	2.41	0.43
Olivine	BO	35	5.19	0.29	3.06	0.41
Mesostasis	BO	36	2.84	0.29	1.70	0.64
Mesostasis	BO	37	4.98	0.28	3.03	0.44
Mesostasis	BO	38	5.92	0.28	4.31	0.40
Pyroxene	chd 6	51	5.32	0.83	4.14	0.98
Pyroxene	chd 6	52	5.15	0.83	3.28	1.08
Olivine	chd 6	53	−6.49	0.81	−6.71	0.92
Olivine	chd 6	54	4.54	0.81	3.83	0.95
Pyroxene	chd 6	55	5.68	0.82	4.66	0.97
Mesostasis	chd 6	56	5.23	0.81	5.19	0.93
Mesostasis	chd 6	57	3.87	0.82	4.58	0.95
Olivine	chd 21	58	0.50	1.81	1.67	1.11
Olivine	chd 21	59	1.31	0.87	3.08	0.96

Table 2. *Continued.* O-isotope composition of chondrule and host object minerals..

Phase	Location	Point	δ18O	2 s.e.	$\delta^{17}O$	2 s.e.
Olivine	chd 21	60	0.93	0.95	2.28	0.99
Pyroxene	chd 21	61	4.44	0.85	3.31	1.10
Pyroxene	chd 21	62	3.90	1.16	2.93	1.33
Pyroxene	chd 21	63	2.19	0.84	2.14	1.20
Mesostasis	chd 21	64	3.43	0.82	4.70	0.94
Mesostasis	chd 21	65	4.25	0.82	5.05	0.94
Olivine	chd x	66	2.79	0.82	0.72	3.89
Olivine	chd x	67	3.22	0.82	2.35	1.00
Pyroxene	chd x	68	3.60	6.75	3.59	1.00
Pyroxene	chd x	69	5.67	0.82	5.13	0.95
Mesostasis	chd x	70	6.96	0.81	7.30	0.93
Mesostasis	chd x	71	6.43	0.81	6.10	0.93

All data given in ‰ and relative to the SMOW standard.

pyroxene or olivine grains and is therefore very different from the compound object studied here. Sokol et al. (2007) reported large (3 mm) clasts in the very primitive Adrar 003 LL(L)3 chondrite, with some of them containing intact BO chondrules. In contrast to their host meteorite, these clasts are strongly metamorphosed and therefore clearly xenolithic. The original textures and compositions of the fragments were largely homogenized during thermal metamorphism on their parent body. To our knowledge, these are the only other clasts hosting BO chondrules reported in the literature. However, these are otherwise very different from the compound object studied here, making the compound object so far unique.

To retain its original BO texture, the chondrule in the compound object must have been in a solid state when it was incorporated into its molten host. We suggest two different formation scenarios. (i) The compound object formed in the solar nebula, when the molten host object collided with a BO chondrule. This scenario then constrains the relative particle velocities and particle temperatures, that is, the collision velocity could not have been high, as otherwise the BO chondrule would not have gotten stuck inside the host object (cf. Arakawa and Nakamoto 2016, 2019; Bogdan et al. 2019). Bogdan et al. (2019) found experimentally that colliding particles at low velocities (<1 m s^{-1}) can fully merge and homogenize, thereby forming macrochondrules. We suggest that the compound object studied here could then represent an intermediate stage between compound and macrochondrule formation. According to the findings of Bogdan et al. (2019), the host object and BO chondrule might have collided with an approximate relative velocity below 1 m s^{-1} and at a temperature above 1200°C.

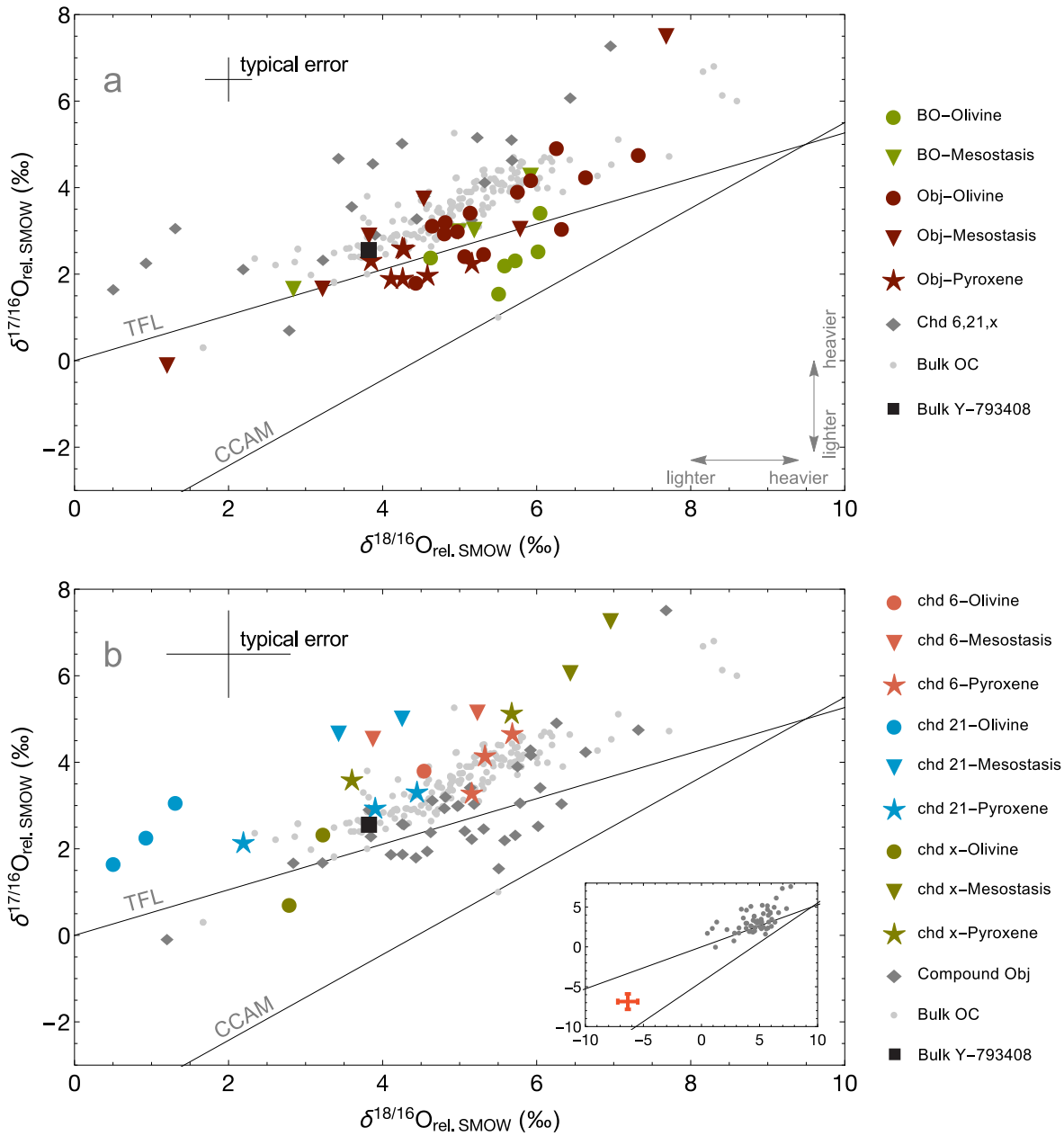

Fig. 5. a) Mineral O-isotope compositions of the compound object. b) Mineral O-isotope compositions of the three other chondrules (cf. Fig. 1). The blue dot in the inset represents one olivine grain in chondrule 6, with significantly lighter O-isotope composition than all other studied mineral grains. Gray dots in the inset represent all measured chondrule mineral values. Gray dots in (a) are the data from the three other chondrules, and gray dots in (b) are the data from the compound object. Black dots represent a selection of ordinary chondrite bulk O-isotope compositions taken from MetBase (2017). Bulk Y-793408 (2.52‰ in $\delta^{17}O$ and 3.87‰ in $\delta^{18}O$) was taken from Kimura et al. (2002). TFL = terrestrial fractionation line; CCAM = carbonaceous chondrite anhydrous mixing line (cf. Young and Russell 1998; Kita et al. 2008). (Color figure can be viewed at wileyonlinelibrary.com.)

Alternatively, (ii) the host object could represent an impact melt that incorporated variable amounts of clastic debris, produced during the impact or collision. The BO chondrule would then represent a piece of such unmelted debris. This scenario is supported by chondrules that occasionally occur as relicts in impact melts, and which were incorporated together with other clasts of the target rock (see fig. 7a of Bischoff et al. [2019] or fig. 4b in Morlok et al. [2017] from the Chelyabinsk melt lithology). However, the large sizes of the individual free-floating olivine grains are atypical when compared to impact melt clast textures described in the literature,

which are usually microporphyritic (e.g., Lunning et al. 2016). It is rather likely that the free-floating olivine grains in the host object are remnants of one or more other chondrules that were added to the host object with which the BO chondrule collided.

Therefore, the first scenario seems more likely, and we suggest that the initial host object was a rare, but not unusual large (macro)chondrule, dominated by significant amounts of mesostasis-like material. We then suggest that the molten host object (mesostasis melting point: ~1100–1200 °C at 1 atm; Andersen 1915) collided with other chondrules at ambient temperatures slightly below the olivine melting point (forsterite: 1800 °C at 1 atm; Kirkpatrick et al. 1983). Chondrules trapped in the host object would then dissolve and their olivines would be scattered throughout the host object. The solid olivine shell surrounding the BO chondrule could have protected this chondrule from dissolving. However, openings in this shell would have allowed exchange of mesostasis material between the host object and the BO chondrule. The identical compositions of mesostasis in the BO chondrule and the host object support material exchange between both mesostases. Alternatively, the homogeneity of BO and host object mesostases is a primary feature. In this case, both mesostases formed at the same time, from the same precursor material and in the same location, thus resulting in the observed chemical similarity.

The free-floating, large, euhedral pyroxene crystals are located at the borders of the host object, and, to a smaller extent, also on the surfaces of the free-floating olivines and the BO chondrule. These sites likely acted as nucleation points of the pyroxenes. The unusually high Al and Ti concentrations in the pyroxenes support in situ crystallization from the Al-, Ti-rich host chondrule melt (see Table 1). Pyroxenes have crystallization temperatures in between olivine and mesostasis, around 1550 °C (at 1 atm; Kirkpatrick et al. 1983). Their large sizes indicate that the compound object was exposed to this temperature for a prolonged time, before it was quenched and the mesostasis formed. This would perfectly agree with the aforementioned scenario in which chondrules were added to, or in combination constituted the initial host object. The chondrules were incorporated and dissolved slightly below the olivine melting point, that is, at temperatures around 1550 °C. This temperature pertained for some time after or during ongoing collisions to allow pyroxene crystallization and, possibly, material exchange between the host object and BO chondrule mesostases. This temperature is also in good agreement with the minimum temperature required to form such objects in experiments (i.e., >1200 °C for macrochondrule formation; Bogdan et al. 2019).

The mesostases in the host object and the BO chondrule have different silica polymorphs: alpha-quartz in the BO chondrule and cristobalite in the host object. Silica is a common, albeit not a frequent constituent of OC chondrules and clasts in OC (e.g., Krot and Wasson 1994; Hezel et al. [2006] and references therein). It usually occurs as tridymite and cristobalite, whereas quartz is rare. The presence of the high-temperature SiO_2 polymorphs in chondrules is typically interpreted to reflect fast cooling (e.g., Hezel et al. 2003, 2006). The cristobalite in the host object might therefore represent fast cooling. The fast temperature drop requires a sudden cool surrounding, as is typical for the fast temperature drop after the chondrule high-T formation event. Alternatively, the host object's mesostasis might have been quenched by the BO chondrule, if the BO chondrule was significantly cooler than the host object during their collision. In this case, the mesostases could not have exchanged material between host object and BO chondrule, nor could the pyroxenes have crystallized on the BO olivine surfaces (cf. Fig. 2). We therefore propose that the host object and the BO chondrule had similar temperatures when they collided, that is, around 1550 °C, as indicated above. The cristobalite in the host object likely formed during the sudden and typical temperature drop shortly after chondrule formation. The olivine shell of the BO chondrule might have slowed cooling of the BO chondrule mesostasis, in which then silica was transformed into alpha-quartz.

O-Isotope Composition of the Compound Object

The oxygen isotope compositions of the phases in the compound object plot mostly in the field of OCs and their chondrules (Fig. 5a; e.g., Clayton et al. 1991; Scott and Krot 2014). A rough estimate of the bulk O-isotope composition of the compound object (using modal recombination) is ~4.9 in $\delta^{18}O$ and ~2.9 in $\delta^{17}O$. This is consistent with an OC origin of the compound object, while a xenolithic origin is unlikely.

The compound object's olivines are ^{18}O-enriched compared to olivines in three additional chondrules measured in Y-793408. The same is true for all phases in the compound object, when comparing these to the whole rock O-isotope composition of Y-793408 (black square in Fig. 5): the $\delta^{18}O$ of all phases in the compound object are shifted toward heavier compositions by up to ~3‰. However, their $\delta^{17}O$ are—within error—mostly identical to bulk Y-793408, thereby indicating some mass-independent O-isotope fractionation of the phases in the compound object.

The mesostases in the BO chondrule and host object are compositionally identical and rich in

refractory elements (Al, Ca, Ti). Refractory material was obviously a major part of the precursor objects that formed the host chondrule. However, only small amounts of CAI material could have been added to the compound object as the oxygen isotope composition of the mesostases plots mostly in the field of OC, and not toward ^{16}O-rich compositions, indicative of CAIs (e.g., Scott and Krot [2014] and references therein). The large amounts of refractory material contributing to the mesostasis likely originated from the same source as all of the material that formed the object studied. However, as some data plot below the terrestrial fractionation line, minor contributions of ^{16}O-rich (e.g., CAI) material cannot be excluded.

The O-isotope composition of the host object mesostasis has a large scatter, bracketed by the lightest and heaviest O-isotope compositions of all the phases. As these compositions plot on a non-mass-dependent trend, these likely reflect some exchange of material with the surrounding gas (e.g., Tissandier et al. 2002; Hezel et al. 2003; Krot et al. 2004; Libourel et al. 2006; Jacquet et al. 2012; Di Rocco and Pack 2015; Friend et al. 2016; Metzler and Pack 2016; Soulié et al. 2017; Ebel et al. 2018; Barosch et al. 2019), that is, an initially lighter material exchanged O-isotopes with a heavier gas, for example, heavy water as found in cosmic symplectites (Sakamoto et al. 2007).

Origin of Ca,Al-Rich Olivine Cores

The Ca,Al-, and Fe-concentration of a few forsteritic olivine cores in the compound object is typical for RF and occurs as free-floating grains next to other individual, but apparently non-refractory olivines. The O-isotope composition of these refractory olivines is, however, similar to typical OC chondrule olivines, and thereby unlike the ^{16}O-enriched isotope compositions of RF (Δ^{17}O between −4 and −10‰; Weinbruch et al. 2000; Pack et al. 2004, 2005). It has been proposed that RF formed by fractional crystallization of refractory condensed melts that experienced gas–melt interactions (Pack et al. 2005). It is since then generally assumed that RF represent ^{16}O-rich relict olivine that crystallized early in the thermal history of chondrules (Pack et al. 2004) or were inherited from chondrule precursors (Jones et al. 2004). However, it has been shown recently that ^{16}O-rich relict chondrule olivine grains are rather Ca-Al-Ti poor (Marrocchi et al. 2018), which is inconsistent with the previous idea that refractory-enriched grains are relicts (Pack and Palme 2003; Pack et al. 2004). Furthermore, Libourel and Portail (2018) and Marrocchi et al. (2018, 2019) suggest that RF formed together with other chondrule olivine grains by epitaxial growth during gas–melt interactions. These RF show constant Δ^{17}O within a single chondrule and between different chondrules, thus reflecting interaction with an ^{16}O-poor gas in the chondrule-forming region (Marrocchi et al. 2018). In the compound object studied here, the RF do not show ^{16}O-rich isotope compositions. This supports our suggestion that all free-floating olivines are in fact remnants of one or more chondrules that collided and constituted the macrochondrule with which the BO chondrule collided.

CONCLUSIONS

We found a unique compound object in Y-793408 (H3.2-an) that is composed of at least two subcomponents. (i) A large host object, likely a mesostasis-rich macrochondrule with individual, free floating, large olivine grains in the mesostasis. Some olivines contain ^{16}O-poor, forsteritic cores. (ii) A BO chondrule trapped in the macrochondrule.

We conclude that the compound object is the fragment of a macrochondrule that collided with and preserved a BO chondrule. If correct, the object appears to be the first macrochondrule with another object still inside it, and thereby provides the first petrographic evidence that compound chondrules and macrochondrules are indeed genetically related, as for example suggested by Bogdan et al. (2019). The object studied therefore allows new insights into macrochondrule formation, their temperature evolution, and details of their formation process.

We suggest that the compound object formed in a nebular setting as follows. First, the mesostasis-rich host object formed by collisions and subsequent merging of molten chondrules, similar to compound chondrule formation (Weyrauch and Bischoff 2012; Bogdan et al. 2019). The free-floating, large olivines represent disaggregated remnants of other chondrules that collided and built the macrochondrule. At least one of these initial chondrules must have consisted of large amounts of mesostasis material, in which the other chondrules dissolved and thereby disintegrated, which then dispersed their olivine grains throughout the macrochondrule. One of the colliding objects was a BO chondrule that got trapped inside the host object, that is, the macrochondrule. The olivines at the BO chondrule's border likely protected the BO chondrule from disintegration. The mesostasis of the BO chondrule possibly exchanged material with the host object, thereby homogenizing both mesostases. During and after these low velocity collisions (<1 m s^{-1}; Bogdan et al. 2019), the macrochondrule remained in a molten state for some time. The temperatures must have been below the forsterite melting point, that is, below

1800 °C, at around the pyroxene crystallization point of 1550 °C (Kirkpatrick et al. 1983), during which the pyroxenes at the border of the host object and some olivines formed. The mesostasis was then quenched, preserving cristobalite in the host object. The BO chondrule mesostasis might have cooled a little slower, maybe due to thermal insulation from the olivine shell, thereby allowing a reconstructive transformation of cristobalite to quartz.

A few of the free-floating olivine grains are RF and likely formed from gas–melt interaction with an ^{16}O-poor gas (Libourel and Portail 2018; Marrocchi et al. 2018, 2019), rather than being relict olivines (e.g., Jones et al. 2004).

Acknowledgments—We would like to thank Addi Bischoff, Natasha Almeida, Claudia Funk, and Marc Chaussidon for helpful discussions and support in the early stage of this work. We thank the National Institute of Polar Research, Japan, for the loan of Y-793408. This research was supported with a grant to D.H. through the Europlanet 2020 RI call for Transnational Access of the European Science Foundation. Europlanet 2020 RI has received funding from the European Union's Horizon 2020 research and innovation programme under grant agreement no. 654208. D.H. gratefully acknowledges funding of this study by the Deutsche Forschungsgemeinschaft (DFG) grants HE 5352/10-1 and PA 346/50-1. J.B. gratefully acknowledges funding by fellowship grant no. GSGS-2019X-02 of the Graduate School of Geosciences, University of Cologne. We thank K. Metzler and S. S. Russell for their thorough and helpful reviews, as well as associate editor G. Benedix for her work.

Editorial Handling—Dr. Gretchen Benedix

REFERENCES

Andersen O. 1915. The system anorthite-forsterite-silica. *American Journal of Science* 232:407–454.

Arakawa S. and Nakamoto T. 2016. Compound chondrule formation via collision of supercooled droplets. *Icarus* 276:102–106.

Arakawa S. and Nakamoto T. 2019. Compound chondrule formation in optically thin shock waves. *The Astrophysical Journal* 877:84–100.

Barosch J., Hezel D. C., Ebel D. S., and Friend P. 2019. Chondrule open system behaviour in ordinary chondrites. *Geochimica et Cosmochimica Acta* 249:1–16.

Bence A. E. and Albee A. L. 1968. Empirical correction factors for the electron micro-analysis of silicates and oxides. *Journal of Geology* 76:382–403.

Bischoff A., Geiger T., Palme H., Spettel B., Schultz L., Scherer P., Schlüter J., and Lkhamsuren J. 1993. Mineralogy, chemistry, and noble gas contents of Adzhi-Bogdo—An LL3-6 chondritic breccia with L-chondritic and granitoidal clasts. *Meteoritics* 28:570–578.

Bischoff A., Scott E. R. D., Metzler K., and Goodrich C. A. 2006. Nature and origins of meteoritic breccias. In *Meteorites and the early solar system II*, edited by Lauretta D. S. and McSween H. Y. Tucson, Arizona: The University of Arizona Press. pp. 679–712.

Bischoff A., Wurm G., Chaussidon M., Horstmann M., Metzler K., Weyrauch M., and Weinauer J. 2017. The Allende multicompound chondrule (ACC)—Chondrule formation in a local super-dense region of the early solar system. *Meteoritics & Planetary Science* 52:906–924.

Bischoff A., Schleiting M., and Patzek M. 2019. Shock stage distribution of 2280 ordinary chondrites—Can bulk chondrites with a shock stage of S6 exist as individual rocks? *Meteoritics & Planetary Science* 54:1–14.

Bogdan T., Teiser J., Fischer N., Kruss M., and Wurm G. 2019. Constraints on compound chondrule formation from laboratory high-temperature collisions. *Icarus* 319:133–139.

Bridges J. C. and Hutchison R. 1997. A survey of clasts and large chondrules in ordinary chondrites. *Meteoritics & Planetary Science* 32:389–394.

Bridges J. C., Franchi I. A., Hutchison R., Morse A. D., Long J. V. P., and Pillinger C. T. 1995. Cristobalite- and tridymite-bearing clasts in Parnallee (LL3) and Farmington (L5). *Meteoritics* 30:715–727.

Clayton R. N., Mayeda T. K., Goswami J. N., and Olsen E. J. 1991. Oxygen isotope studies of ordinary chondrites. *Geochimica et Cosmochimica Acta* 55:2317–2337.

Corrigan C. M., Lunning N. G., and Ziegler K. 2015. An H chondrite melt clast in an LL chondrite: Evidence for mixing of ordinary chondrite parent bodies (abstract #2678). 46th Lunar and Planetary Science Conference. CD-ROM.

Crowther S. A., Filtness M. J., Jones R. H., and Gilmour J. D. 2018. Old formation ages of igneous clasts on the L chondrite parent body reflect an early generation of planetesimals or chondrule formation. *Earth and Planetary Science Letters* 481:372–386.

Di Rocco T. D. and Pack A. 2015. Triple oxygen isotope exchange between chondrule melt and water vapor: An experimental study. *Geochimica et Cosmochimica Acta* 164:17–34.

Ebel D. S., Alexander C. M.O'D., and Libourel G. 2018. Vapor-melt exchange—Constraints on chondrite formation conditions and processes. In *Chondrules: Records of protoplanetary disk processes*, edited by Russell S. S., Connolly Jr. H. C., and Krot A. N. Cambridge, UK: Cambridge University Press. pp. 151–174.

Etchepare J., Merian M., and Smetankine L. 1974. Vibrational normal modes of SiO2. I. a- and b-quartz. *The Journal of Chemical Physics* 60:1873–1876.

Etchepare J., Merian M., and Kaplan P. 1978. Vibrational normal modes of SiO_2 II. Cristobalite and tridymite. *The Journal of Chemical Physics* 68:1531–1537.

Friend P., Hezel D. C., and Mucerschi D. 2016. The conditions of chondrule formation, Part II: Open system. *Geochimica et Cosmochimica Acta* 173:198–209.

Gattacceca J., Krzesinska A., Marrocchi Y., Meier M. M. M., Bourot-Denise M., and Lenssen R. 2017. Asteroid mixing revealed by NWA 5764, a polymict LL breccia with L clasts. *Meteoritics & Planetary Science* 52:2289–2304.

Herd C. D., Friedrich J. M., Greenwood R. C., and Franchi I. A. 2013. An igneous-textured clast in the Peace River

meteorite: Insights into accretion and metamorphism of asteroids in the early solar system. *Canadian Journal of Earth Sciences* 50:14–25.

Hewins R. H., Connolly H. C. Jr., Lofgren G. E., and Libourel G. 2005. Experimental constraints on chondrule formation. In *Chondrites and the protoplanetary disk*, vol. 341, edited by Krot A. N., Scott E. R. D., and Reipurth B. San Francisco, California: Astronomical Society of the Pacific Press. pp. 286–316.

Hezel D. C., Palme H., Brenker F. E., and Nasdala L. 2003. Evidence for fractional condensation and reprocessing at high temperatures in CH-chondrites. *Meteoritics & Planetary Science* 38:1199–1216.

Hezel D. C., Palme H., Nasdala L., and Brenker F. E. 2006. Origin of SiO_2-rich components in ordinary chondrites. *Geochimica et Cosmochimica Acta* 70:1548–1564.

Hutchison R., Williams C. T., Din V. K., Clayton R. N., Kirschbaum C., Paul R. L., and Lipschutz M. E. 1988. A planetary, H-group pebble in the Barwell, L6, unshocked chondritic meteorite. *Earth and Planetary Science Letters* 90:105–118.

Jacquet E., Alard O., and Gounelle M. 2012. Chondrule trace element geochemistry at the mineral scale. *Meteoritics & Planetary Science* 47:1695–1714.

Jones R. H., Leshin L. A., Guan Y., Sharp Z. D., Durakiewicz T., and Schilk A. J. 2004. Oxygen isotope heterogeneity in chondrules from the Mokoia CV3 carbonaceous chondrite. *Geochimica et Cosmochimica Acta* 68:3423–3438.

Kimura M., Hiyagon H., Palme H., Spettel B., Wolf D., Clayton R. N., Mayeda T. K., Sato T., Suzuki A., and Kojima H. 2002. Yamato 792947, 793408 and 82038: The most primitive H chondrites, with abundant refractory inclusions. *Meteoritics & Planetary Sciences* 37:1417–1434.

Kirkpatrick R. J., Reck B. H., Pelly I. Z., and Kuo L.-C. 1983. Programmed cooling experiments in the system MgO-SiO_2: Kinetics of a peritectic reaction. *American Mineralogist* 68:1905–1983.

Kita N. T., Kimura M., Ushikubo T., Valley J. W., and Nyquist L. E. 2008. Oxygen isotope systematics of chondrules from the least equilibrated H chondrite (abstract #2059). 39th Lunar and Planetary Science Conference.

Krot A. N. and Wasson J. T. 1994. Silica-merrihueite/roedderite-bearing chondrules and clasts in ordinary chondrites: New occurrences and possible origin. *Meteoritics* 29:707–718.

Krot A. N., Libourel G., Goodrich C., and Petaev M. I. 2004. Silica-igneous rims around magnesian chondrules in CR carbonaceous chondrites: Evidence for fractional condensation during chondrule formation. *Meteoritics & Planetary Science* 39:1931–1955.

Libourel G. and Portail M. 2018. Chondrules as direct thermochemical sensors of solar protoplanetary disk gas. *Science Advances* 4:eaar3321.

Libourel G., Krot A. N., and Tissandier L. 2006. Role of gas–melt interaction during chondrule formation. *Earth and Planetary Science Letters* 251:232–240.

Lunning N. G., Corrigan C. M., McSween H. Y., Tenner T. J., Kita N. T., and Bodnar R. J. 2016. CV and CM chondrite impact melts. *Geochimica et Cosmochimica Acta* 189:338–358.

Marrocchi Y., and Chaussidon M. 2015. A systematic for oxygen isotopic variation in meteoritic chondrules. *Earth and Planetary Science Letters* 430:308–315.

Marrocchi Y., Villeneuve J., Batanova V., Piani L., and Jacquet E. 2018. Oxygen isotopic diversity of chondrule precursors and the nebular origin of chondrules. *Earth and Planetary Science Letters* 496:132–141.

Marrocchi Y., Euverte R., Villeneuve J., Batanova V., Welsch B., Ferriere L., and Jacquet E. 2019. Formation of CV chondrules by recycling of amoeboid olivine aggregate-like precursors. *Geochimica et Cosmochimica Acta* 247:121–141.

MetBase: Meteorite Information Database. 2017. GeoPlatform UG. http://www.metbase.org

Metzler K. and Pack A. 2016. Chemistry and oxygen isotopic composition of cluster chondrite clasts and their components in LL 3 chondrites. *Meteoritics & Planetary Science* 51:276–302.

Metzler K., Bischoff A., Greenwood R. C., Palme H., Gellissen M., Hopp J., Franchi I. A., and Trieloff M. 2011. The L3–6 chondritic regolith breccia Northwest Africa (NWA) 869:(I) Petrology, chemistry, oxygen isotopes, and Ar-Ar age determinations. *Meteoritics & Planetary Science* 46:652–680.

Morlok A., Bischoff A., Patzek M., Sohn M., and Hiesinger H. 2017. Chelyabinsk – A rock with many different (stony) faces: An infrared study. *Icarus* 284:431–442.

Nasdala L., Wopenka B., Lengauer C. L. 2004. Discussion on: transformation of SiO^2 to the amorphous state by shearing at high pressure by Furuichi et al (2003, vol. 88:926–928). *American Mineralogist* 89:912–913.

Pack A. and Palme H. 2003. Partitioning of Ca and Al between forsterite and silicate melt in dynamic systems with implications for the origin of Ca, Al-rich forsterites in primitive meteorites. *Meteoritics & Planetary Science* 38:1263–1281.

Pack A., Yurimoto H., and Palme H. 2004. Petrographic and oxygen-isotopic study of refractory forsterites from R.-chondrite Dar Al Gani 013 (R3. 5–6), unequilibrated ordinary and carbonaceous chondrites. *Geochimica et Cosmochimica Acta* 68:1135–1157.

Pack A., Palme H., and Shelley J. M. G. 2005. Origin of chondritic forsterite grains. *Geochimica et Cosmochimica Acta* 69:3159–3182.

Piani L., Marrocchi Y., Libourel G., and Tissandier L. 2016. Magmatic sulfides in the porphyritic chondrules of EH enstatite chondrites. *Geochimica et Cosmochimica Acta* 195:84–99.

Prinz M., Nehru C. E., Weisberg M. K., Delaney J. S., Yanai K., and Kojima H. 1984. H chondritic clasts in a Yamato L6 chondrite: Implications for metamorphism. *Meteoritics* 19:292–293.

Rubin A. E., Breen J. P., Isa J., and Tutorow S. 2017. NWA 10214—An LL3 chondrite breccia with an assortment of metamorphosed, shocked, and unique chondrite clasts. *Meteoritics & Planetary Science* 52:372–390.

Ruzicka A., Kring D. A., Hill D. H., Boynton W. V., Clayton R. N., and Mayeda T. K. 1995. Silica-rich orthopyroxenite in the Bovedy chondrite. *Meteoritics* 30:57–70.

Sakamoto N., Seto Y., Itoh S., Kuramoto K., Fujino K., Nagashima K., Krot A. N., and Yurimoto H. 2007. Remnants of the early solar system water enriched in heavy oxygen isotopes. *Science* 317:231–233.

Scott E. R. D. and Krot A. N. 2014. Chondrites and their components. In *Treatise on geochemistry*, 2nd ed., edited by H. Holland and K. Turekian. Oxford, UK: Elsevier. pp. 65–137.

Scott J. F. and Porto S. P. S. 1967. Longitudinal and transversal optical lattice vibrations in quartz. *Physical Review* 161:903–910.

Sokol A. K., Bischoff A., Marhas K. K., Mezger K., and Zinner E. 2007. Late accretion and lithification of chondritic parent bodies: Mg isotope studies on fragments from primitive chondrites and chondritic breccias. *Meteoritics & Planetary Science* 42:1291–1308.

Soulié C., Libourel G., and Tissandier L. 2017. Olivine dissolution in molten silicates: an experimental study with application to chondrule formation. *Meteoritics & Planetary Science* 52:225–250.

Steele I. M. 1986. Compositions and textures of relic forsterite in carbonaceous and unequilibrated ordinary chondrites. *Geochimica et Cosmochimica Acta* 50:1379–1395.

Terada K. and Bischoff A. 2009. Asteroidal granite-like magmatism 4.53 Gyr ago. *The Astrophysical Journal* 699: L68–L71.

Tissandier L., Libourel G., and Robert F. 2002. Gas-melt interactions and their bearing on chondrule formation. *Meteoritics & Planetary Science* 37:1377–1389.

Wasson J. T., Krot A. N., Lee M. S., and Rubin A. E. 1995. Compound chondrules. *Geochimica et Cosmochimica Acta* 59:1847–1869.

Weinbruch S., Palme H., and Spettel B. 2000. Refractory forsterite in primitive meteorites: Condensates from the solar nebula? *Meteoritics & Planetary Science* 35:161–171.

Weisberg M. K., Prinz M., and Nehru C. E. 1988. Macrochondrules in ordinary chondrites: Constraints on chondrule-forming processes. *Meteoritics* 23:309–310.

Weyrauch M. and Bischoff A. 2012. Macrochondrules in chondrites-formation by melting of mega-sized dust aggregates and/or by rapid collisions at high temperatures? *Meteoritics & Planetary Science* 47:2237–2250.

Yokoyama T., Misawa K., Okano O., Shih C. Y., Nyquist L. E., Simon J. I., Tappa M. J., and Yoneda S. 2017. Extreme early solar system chemical fractionation recorded by alkali-rich clasts contained in ordinary chondrite breccias. *Earth and Planetary Science Letters* 458:233–240.

Young E. D. and Russell S. S. 1998. Oxygen reservoirs in the early solar nebula inferred from an Allende CAI. *Science* 282:452–455.